# Supplementary Information

# Heterodimetallic [LnLn'] Lanthanide Complexes: Towards a Chemical Design of 2-Qubit Molecular Spin Quantum Gates

David Aguilà, Leoní A. Barrios, Verónica Velasco, Olivier Roubeau, Ana Repollés, Pablo J. Alonso, Javier Sesé, Simon J. Teat, Fernando Luis* and Guillem Aromí*

**Table of contents** page number

**A spin Hamiltonian for a pair of weakly coupled rare-earth Kramers ions**

We propose a straightforward extension of the fictitious spin formalism, often used to describe the magnetic response of a Kramers doublet, to the case of two coupled Kramers ions. Within the lowest lying multiplet, defined by a total angular momentum *J*, the magnetic properties of a lanthanide ion can be described by the following Hamiltonian

$$\mathrm{H} = \sum_{p} \sum_{q=-p}^{+p} B_p^q O_p^q(\mathbf{J}) - g_J \mu_\mathrm{B} \mathbf{H}\mathbf{J} \qquad (1)$$

The first term in Eq. (1) arises from the interaction of 4*f* electrons with the crystal field and is written in terms of effective operators that involve powers of different angular momentum components. The coefficients $B_p^q$ are the anisotropy parameters. The second term is the Zeeman interaction with a magnetic field **H**, where $g_J$ is an effective gyromagnetic ratio.

In the case of a Kramers ion, energy levels are, at least, doubly degenerate. If there are no additional degeneracies, the ground level defines a two-dimensional subspace. For any state $\Phi$ of this subspace, the pair $\{\Phi,\mathrm{T}\Phi\}$, where T is the time-reversal operator, defines a suitable basis, usually referred to as a Kramers conjugate state basis (KCSB). Provided that both the thermal energy $k_\mathrm{B}T$ and the Zeeman splitting are small enough in comparison with the crystal field splitting $\Delta$ between the ground and first excited Kramers doublets, the magnetic response can be described with an effective $S$ = 1/2 system in a magnetic field, using the following Hamiltonian

$$\mathrm{H}^S = \mu_B \mathbf{H} \cdot \tilde{g} \cdot \mathbf{S} \qquad (2)$$

where $\tilde{g}$ is an anisotropic *g*-tensor. The EPR spectrum supplies information about the principal values and principal directions of this tensor.[1] It is, however, important to remember that only absolute values can be obtained from conventional EPR experiments; the sign of the product of the three principal values can be determined by using a circularly polarized microwave.[2]

[1] Poole, C.P. Jr., Farach H. *Theory of Magnetic Resonance*. Wiley-Interscience (N.Y., 1972) chapter 6.

[2] Abragam A., Bleaney B. *Electron Paramagnetic Resonance of Transitions Ions*. Oxford University Press (Oxford UK, 1970), chapter 3

Let us now consider *two* lanthanide Kramers ions, (1) and (2). The Hamiltonian of the combined system is given by:

$$\mathrm{H} = \mathrm{H}_1 + \mathrm{H}_2 + \mathrm{H}_{12} \tag{3}$$

where $\mathrm{H}_r$ ($r$ = 1,2) are the spin Hamiltonians of each of the two isolated ions

$$\mathrm{H}_r = \sum_p \sum_{q=-p}^{+p} B_p^q(r) O_p^q(\mathbf{J}_r) - g_{J,r}\mu_\mathrm{B}\mathbf{H}\mathbf{J}_r \tag{4}$$

and $\mathrm{H}_{12}$ accounts for their mutual interactions. The zeroth-order Hamiltonian corresponds to considering both systems without mutual interaction, i.e. $\mathrm{H}_{12} = 0$. The zeroth-order solutions of (3) are then given by $|\Psi\rangle = |\Phi_1\rangle \otimes |\Phi_2\rangle$, where each $|\Phi_r\rangle$ is solution of $\mathrm{H}_r|\Phi_r\rangle = E_r|\Phi_r\rangle$ ($r$ = 1, 2), and have energies $E = E_1 + E_2$. If there are no accidental degeneracies, these levels have fourfold degeneracy and admit a basis given by $\{|\Phi_1\rangle \otimes |\Phi_2\rangle$, $|\Phi_1\rangle \otimes |\mathrm{T}_2\Phi_2\rangle$, $|\mathrm{T}_1\Phi_1\rangle \otimes |\Phi_2\rangle$, $|\mathrm{T}_1\Phi_1\rangle \otimes |\mathrm{T}_2\Phi_2\rangle\}$.

Interactions split the ground level and give rise to energy eigenstates that are linear combinations of the basis states. We next consider their effect by introducing a bilinear coupling between the angular momenta of ions (1) and (2)

$$\mathrm{H}_{12} = \mathbf{J}_1 \tilde{C} \mathbf{J}_2 \tag{5}$$

where $\tilde{C}$ is a second rank tensor. This form includes a dipole-dipole interaction as well as any exchange interaction. For instance, in the case of a Heisenberg isotropic exchange $\tilde{C}$ reduces to a constant $J_{\mathrm{ex}}$. If the interaction $\mathrm{H}_{12}$ is sufficiently weak as compared with $\mathrm{H}_1 + \mathrm{H}_2$, its effect can be treated using first-order perturbation theory within each of the subspaces associated with eigenstates of $\mathrm{H}_1 + \mathrm{H}_2$. At low enough temperatures, the magnetic properties can then be described by two coupled effective spins $S_1 = S_2 = ½$, with the correspondence $g_{J,r}\mathbf{J}_r \rightarrow \tilde{g}_r \mathbf{S}_r$. The effective Hamiltonian is then given by

$$\mathrm{H}^{S_1,S_2} = \mu_B \mathbf{H} \tilde{g}_1 \mathbf{S}_1 + \mu_B \mathbf{H} \tilde{g}_2 \mathbf{S}_2 + \mathbf{S}_1 \tilde{D} \mathbf{S}_2 \tag{6}$$

where $\tilde{D}$ is a coupling tensor given by

$$\tilde{D} = \frac{1}{g_{J1} g_{J2}} \left( \tilde{g}_1 \tilde{C} \tilde{g}_2 \right) \tag{7}$$

And $\tilde{g}_1$ and $\tilde{g}_2$ are, respectively, the effective $g$-tensors for the description of the ground Kramers doublet of ions (1) and (2). In general, $\tilde{D}$ is anisotropic and

non-symmetric. It becomes symmetric if $\widetilde{C}$ is a scalar, i.e. for a Heisenberg interaction between $\mathbf{J}_1$ and $\mathbf{J}_2$, and if the principal axes of $\widetilde{g}_1$ and $\widetilde{g}_2$ are collinear. A similar solution was derived previously for a particular case.[3] In the calculations shown in Fig. 3 of the main text, we took $\widetilde{C} = J_{12}$, thus scalar, but considered a 70 degrees rotation of the principal axes of ion 2 around the $\mathbf{x}_1 = \mathbf{x}_2$ axis.

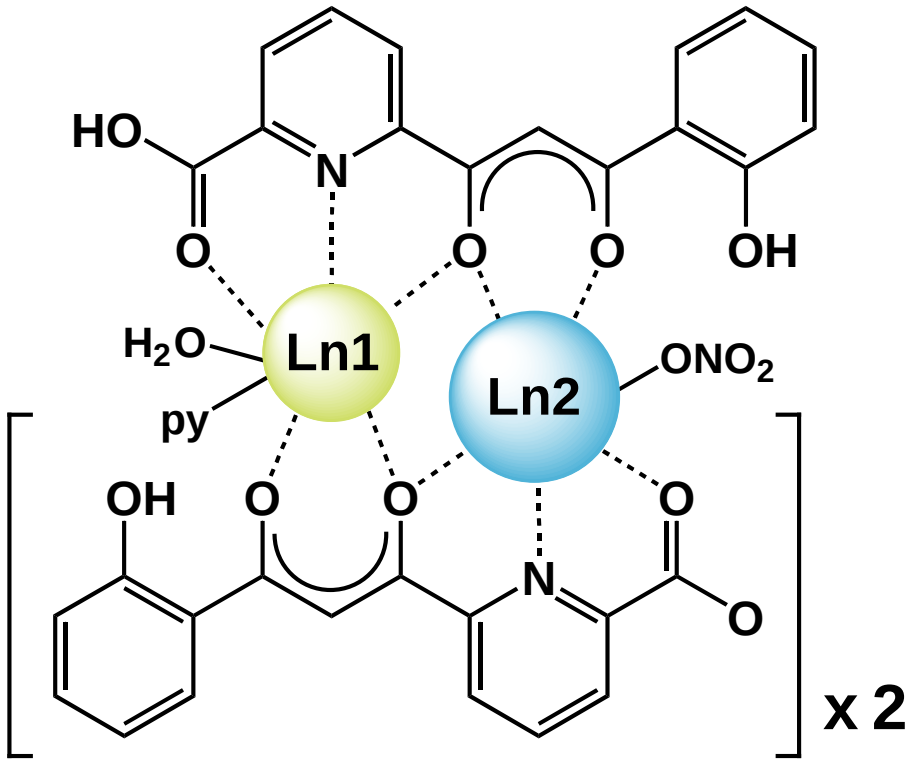


**Figure S1.** Schematic representation of the structure of complexes $[LnLn'(HL)_2(H_2L)(NO_3)(py)(H_2O)]$ (**1** and **4** to **7**), emphasizing the difference between smaller coordinating *site 1* (two 'O,O' and one 'O,N,O' coordination poket) and larger cavity *site 2* (one 'O,O' and two 'O,N,O' coordination pokets).

[3] Palii A.V., Tsukerblat B.S., Coronado E., Clemente-Juan J.M., Morrás-Almenar J.J. *Inorg. Chem*. **2003**, *42*, 2455-2458.

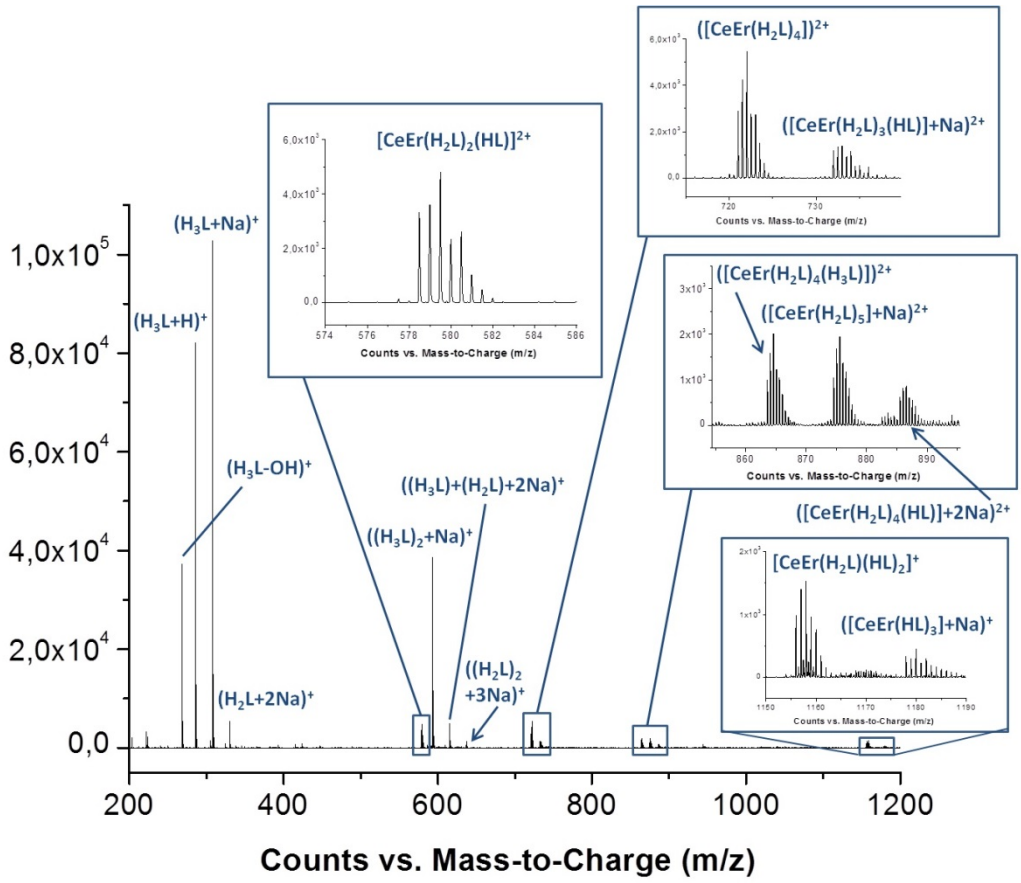


**Figure S2.** Positive-ion ESI mass spectrogram of $[CeEr(HL)_2(H_2L)(NO_3)(py)(H_2O)]$ (**1**), emphasizing the heterometallic fragments.

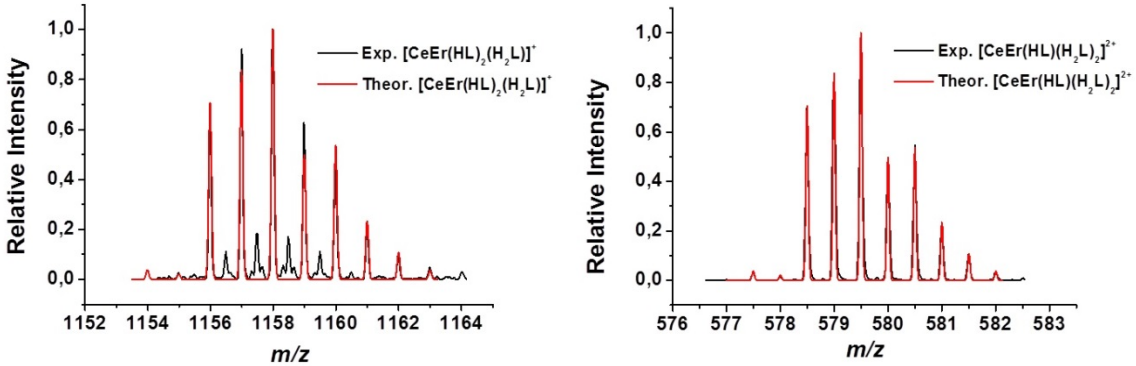


**Figure S3.** Comparison of two representative peaks from the positive-ion ESI mass spectrogram of $[CeEr(HL)_2(H_2L)(NO_3)(py)(H_2O)]$ (**1**), with their simulated ones, were the isotopic distribution has been taken into account.

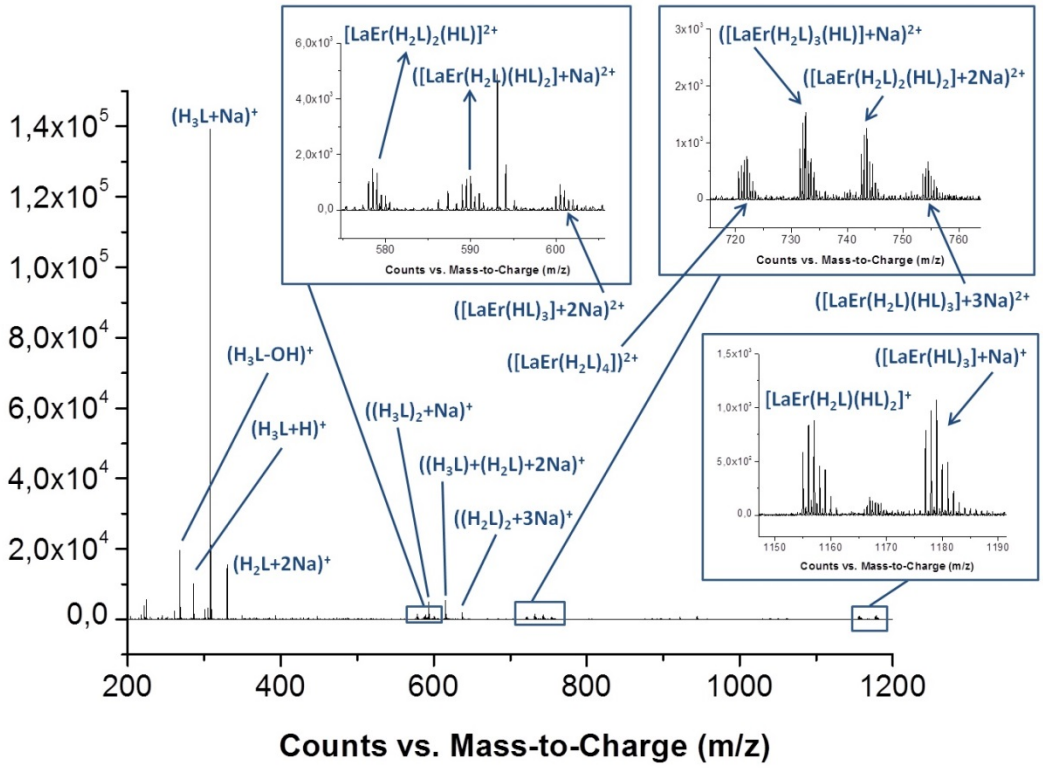


**Figure S4.** Positive-ion ESI mass spectrogram of $[LaEr(HL)_2(H_2L)(NO_3)(py)(H_2O)]$ (**4**), emphasizing the heterometallic fragments.

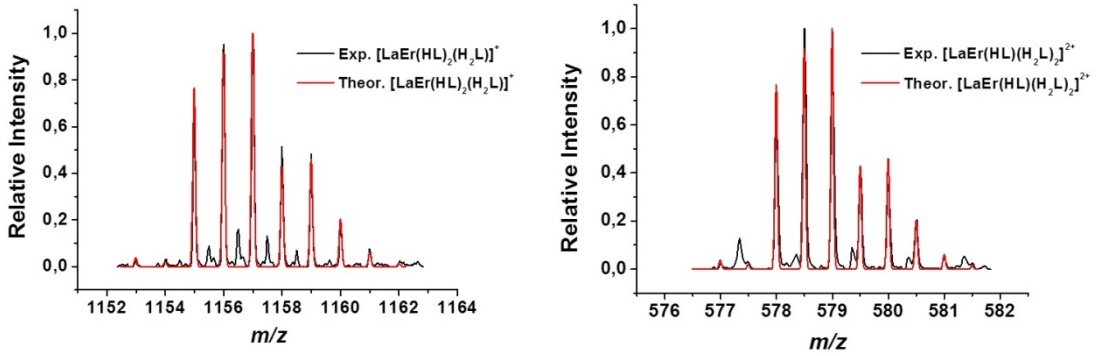


**Figure S5.** Comparison of two representative peaks from the positive-ion ESI mass spectrogram of $[LaEr(HL)_2(H_2L)(NO_3)(py)(H_2O)]$ (**4**), with their simulated ones, were the isotopic distribution has been taken into account.

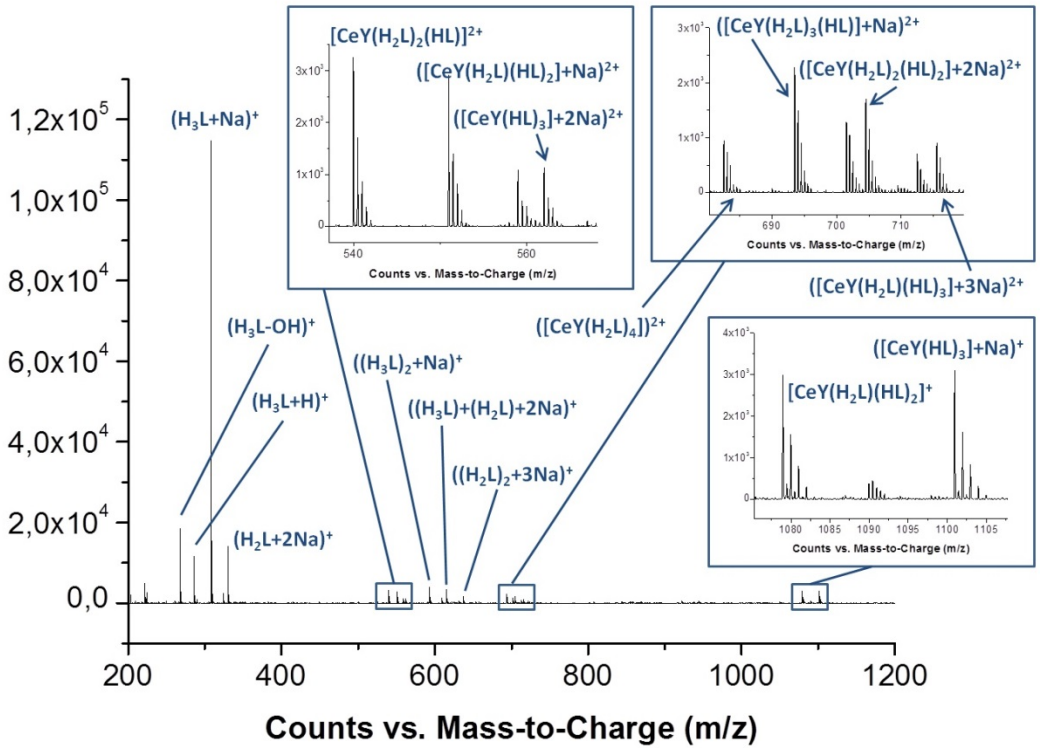


**Figure S6.** Positive-ion ESI mass spectrogram of $[CeY(HL)_2(H_2L)(NO_3)(py)(H_2O)]$ (**5**), emphasizing the heterometallic fragments.

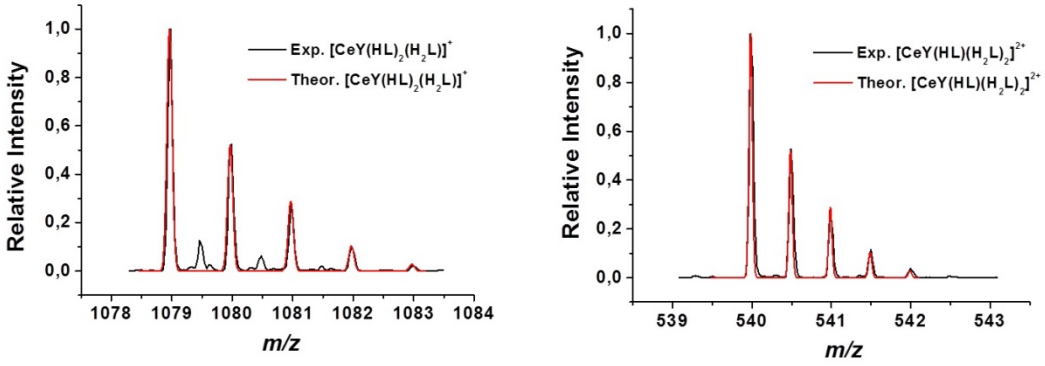


**Figure S7.** Comparison of two representative peaks from the positive-ion ESI mass spectrogram of $[CeY(HL)_2(H_2L)(NO_3)(py)(H_2O)]$ (**5**), with their simulated ones, were the isotopic distribution has been taken into account.

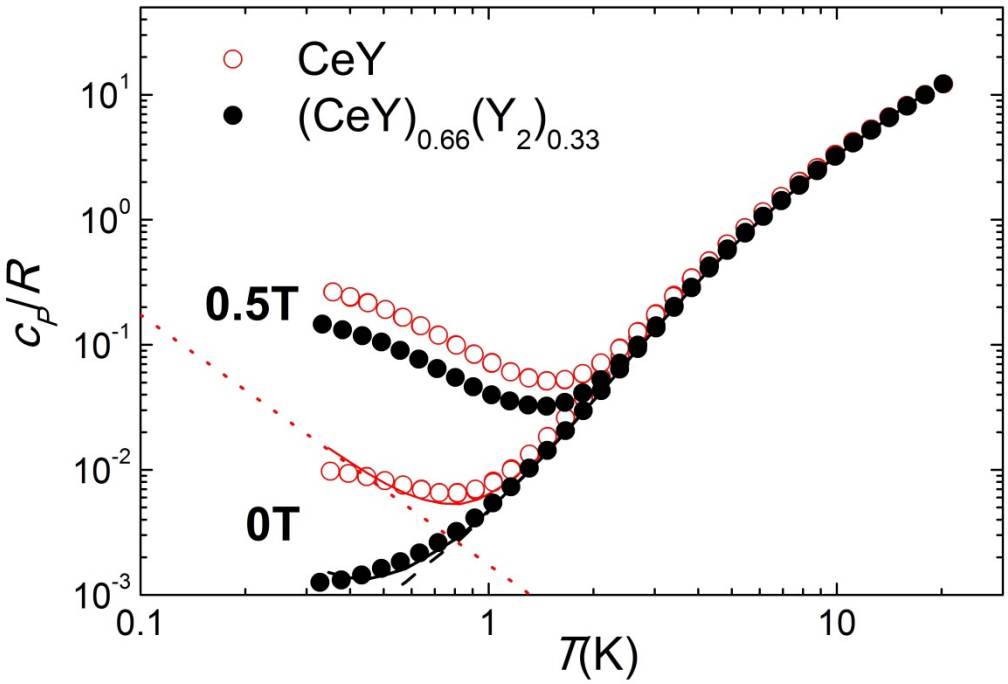


**Figure S8. Heat capacity of individual qubits.** Specific heat data of powder samples of pure [CeY] (complex **5**) and magnetically diluted $[CeY]_{0.7}[Y_2]_{0.3}$ (complex **6**) measured at zero field and under an applied magnetic field $\mu_0 H$ = 0.5 T. The specific heat of the diamagnetic complex [LaY] is also shown, as it provides the contribution $c_{latt}$ of vibrational modes to $c_P$. The dashed line is a high temperature series $\frac{c_{dipolar}}{R} \approx \frac{\mu_{eff}^2 \langle H_{dip}^2 \rangle}{2(k_B T)^2}$, where $\mu_{eff}$ = 1.9 $\mu_B$ is the low-$T$ effective magnetic moment extracted from the equilibrium susceptibility, and $\langle H_{dip}{}^2 \rangle$ is the average square dipolar magnetic field seen by each molecule. We find $\langle H_{dip}{}^2 \rangle \approx (45\ \text{mT})^2$ and $\langle H_{dip}{}^2 \rangle \approx (15\ \text{mT})^2$ for, respectively, pure [CeY] and $[CeY]_{0.7}[Y_2]_{0.3}$. For magnetic fields much stronger than the typical $H_{dip}$, specific heat curves measured on samples with different concentrations of spins simply scale with $x$ (molar fraction of magnetic molecules), showing that the effect of intermolecular couplings becomes then negligible.

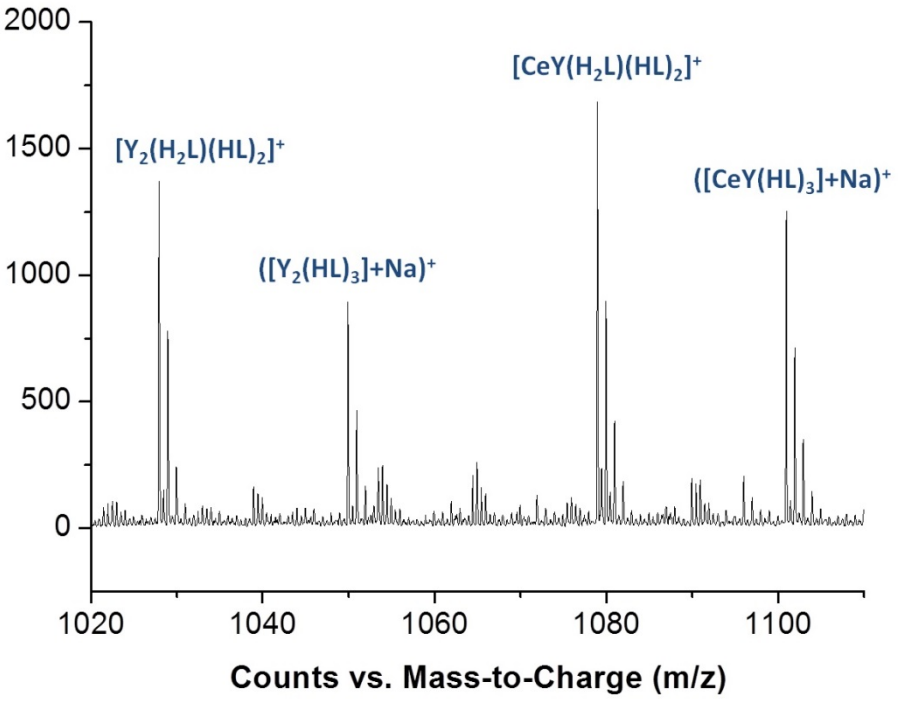


**Figure S9.** Representative region of the positive-ion ESI mass spectrogram of $[CeY(HL)_2(H_2L)(NO_3)(py)(H_2O)]_{0.7}[Y_2(HL)_2(H_2L)(NO_3)(py)(H_2O)]_{0.3}$ (**6**), showing fragments of the $[Y_2]$ and the [CeY] species, while the $[Ce_2]$ complex could not be observed.

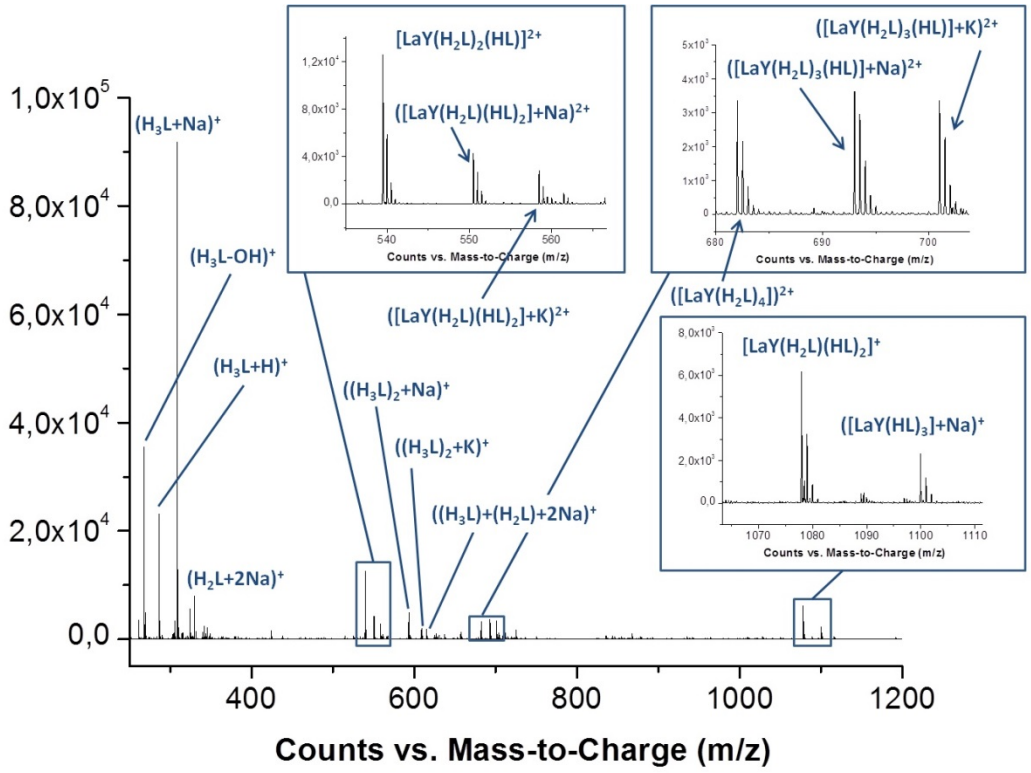


**Figure S10.** Positive-ion ESI mass spectrogram of $[LaY(HL)_2(H_2L)(NO_3)(py)(H_2O)]$ (**7**), emphasizing the heterometallic fragments.

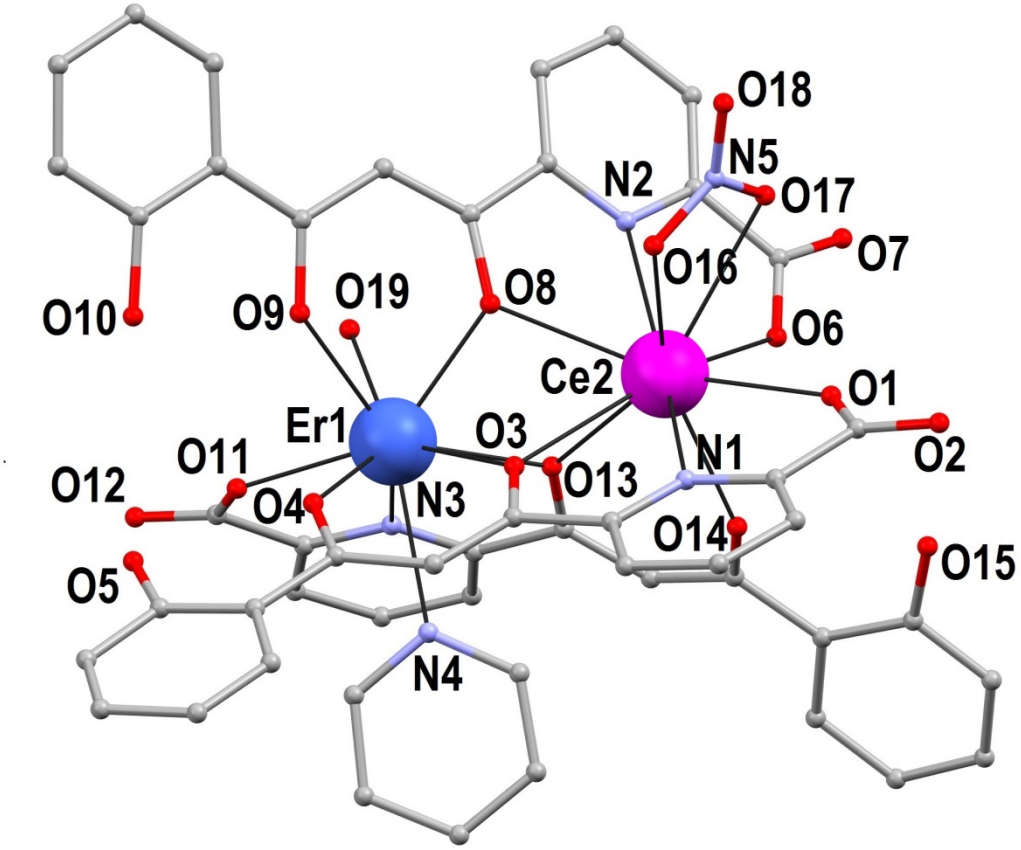


**Figure S11.** Representation of the molecular structure of $[CeEr(HL)_2(H_2L)(NO_3)(py)(H_2O)]$ (**1**). Only heteroatoms are labelled. Carbon atoms are in grey. Hydrogen atoms are not shown for clarity.

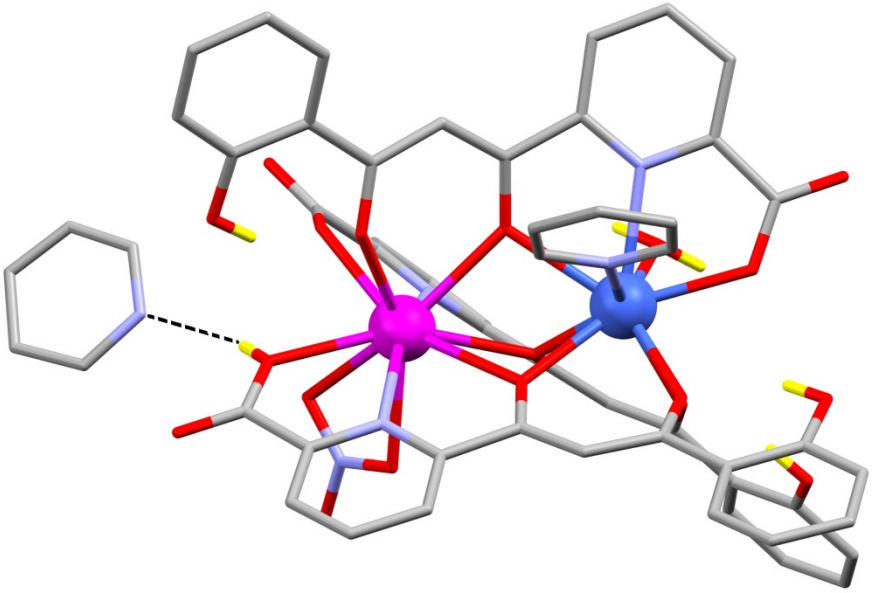

**Figure S12.** Representation of $[CeEr(HL)_2(H_2L)(NO_3)(py)(H_2O)]$ (**1**) emphasizing the H-bond (dashed line) formed between one molecule of pyridine and the protonated carboxylate moiety from the $H_2L^-$ ligand.

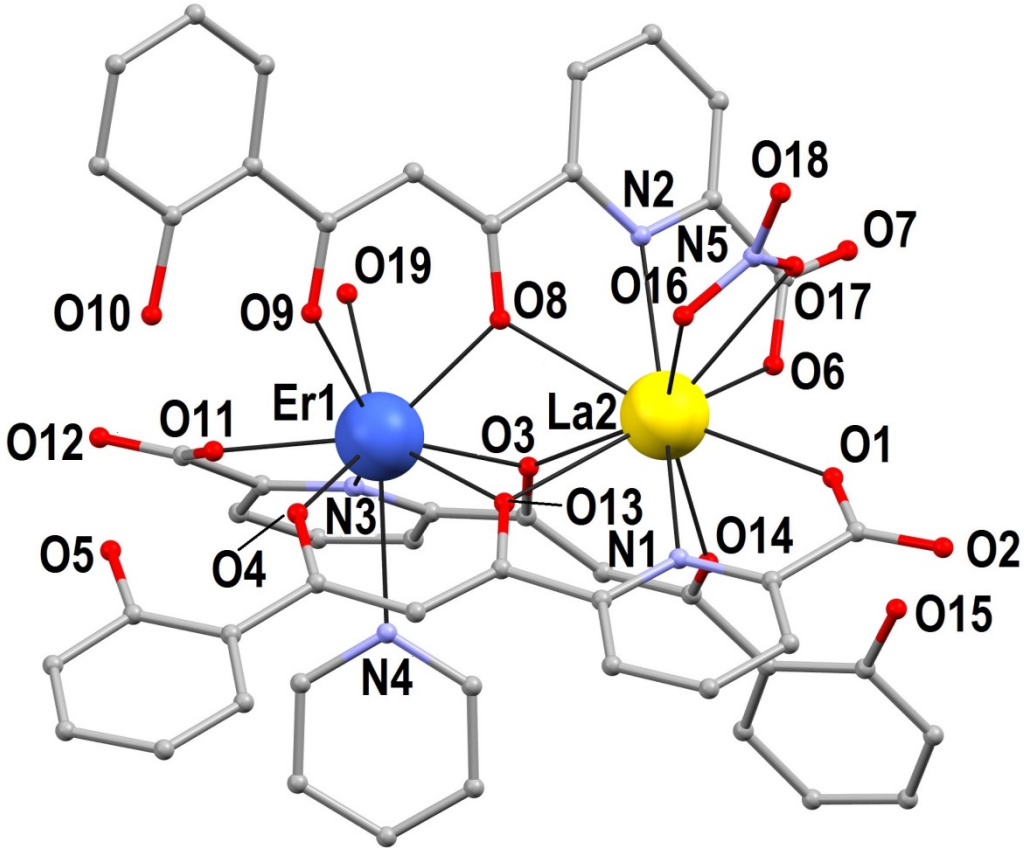


**Figure S13.** Representation of the molecular structure of $[LaEr(HL)_2(H_2L)(NO_3)(py)(H_2O)]$ (**4**). Only heteroatoms are labelled. Carbon atoms are in grey. Hydrogen atoms are not shown for clarity.

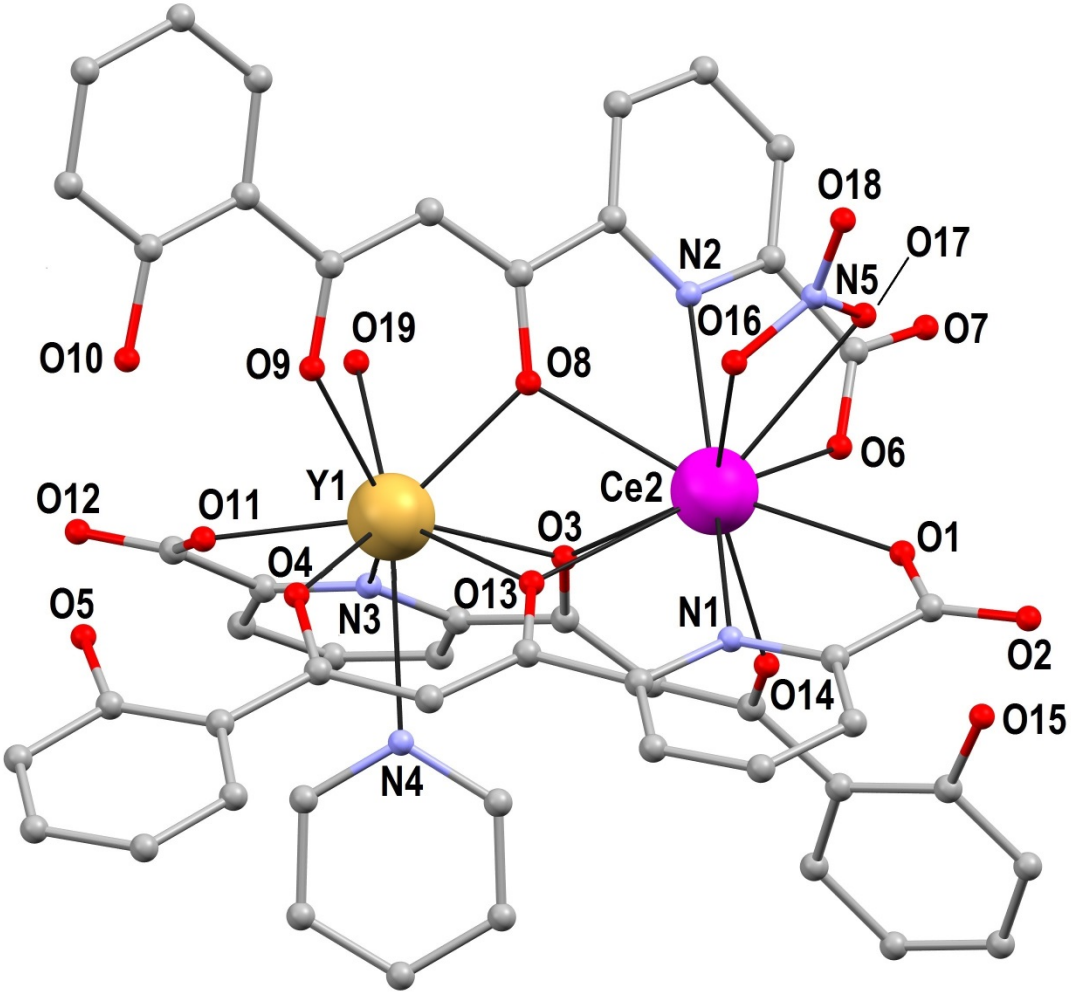


**Figure S14.** Representation of the molecular structure of $[CeY(HL)_2(H_2L)(NO_3)(py)(H_2O)]$ (**5**). Only heteroatoms are labelled. Carbon atoms are in grey. Hydrogen atoms are not shown for clarity.

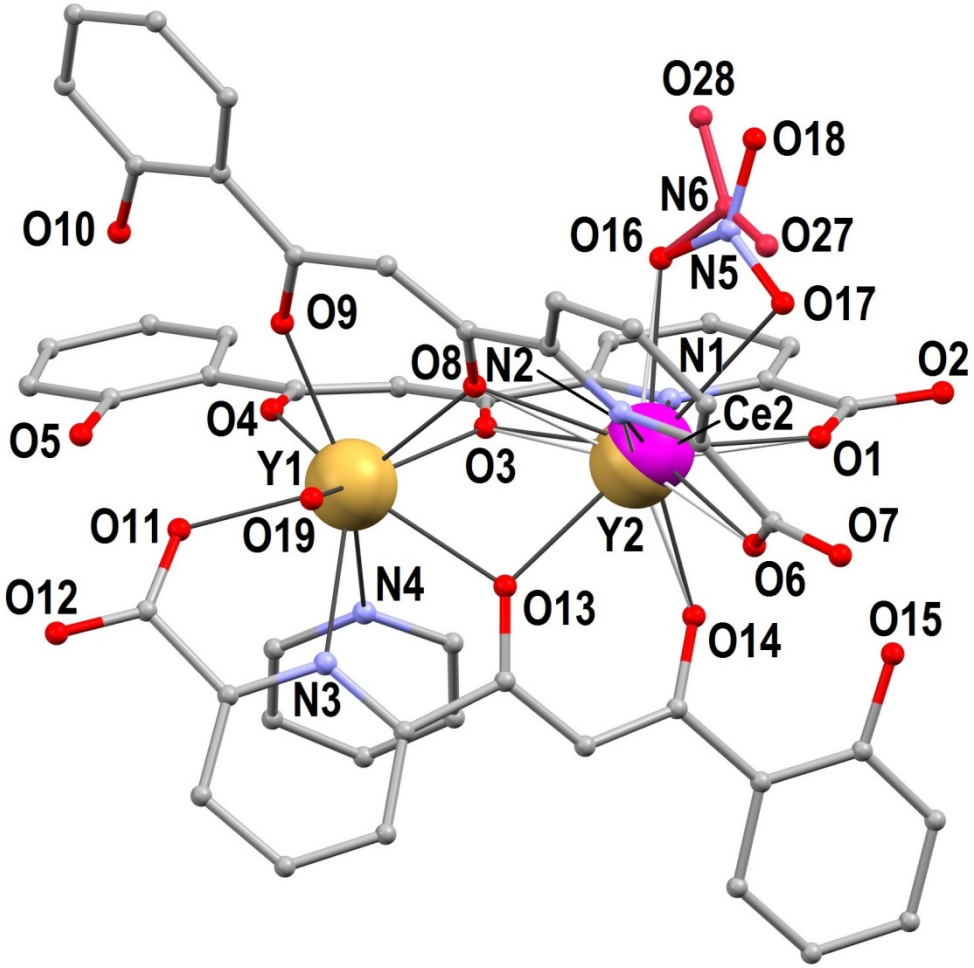


**Figure S15.** Representation of the molecular structure of $[(Ce_{0.7}Y_{0.3})Y(HL)_2(H_2L)(NO_3)(py)(H_2O)]$ (**6**). The both atoms occupying the position of Ln2 (either Ce2 or Y2) are shown as well as both positions of $NO_3^-$ corresponding to each of these occupations. Only heteroatoms are labelled. Carbon atoms are in grey. Hydrogen atoms are not shown for clarity.

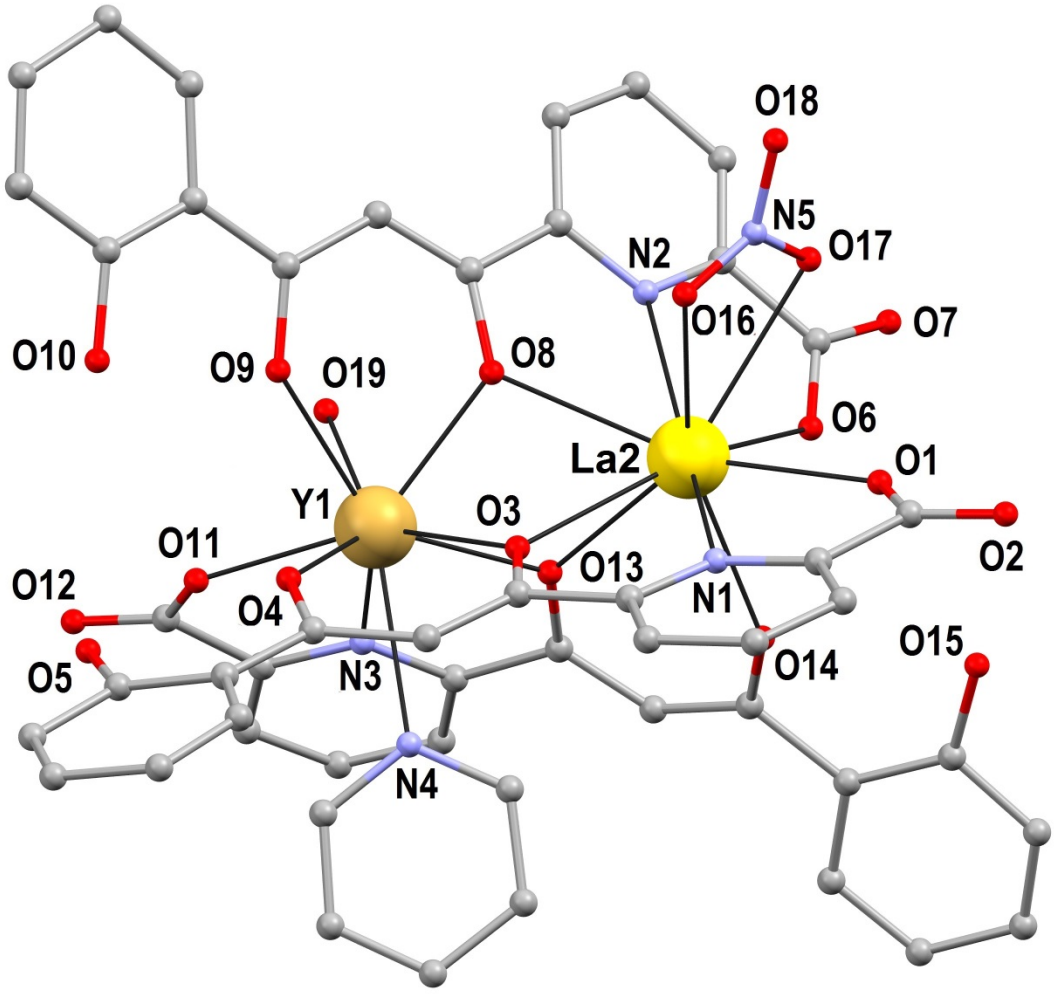


**Figure S16.** Representation of the molecular structure of $[LaY(HL)_2(H_2L)(NO_3)(py)(H_2O)]$ (**7**). Only heteroatoms are labelled. Carbon atoms are in grey. Hydrogen atoms are not shown for clarity.

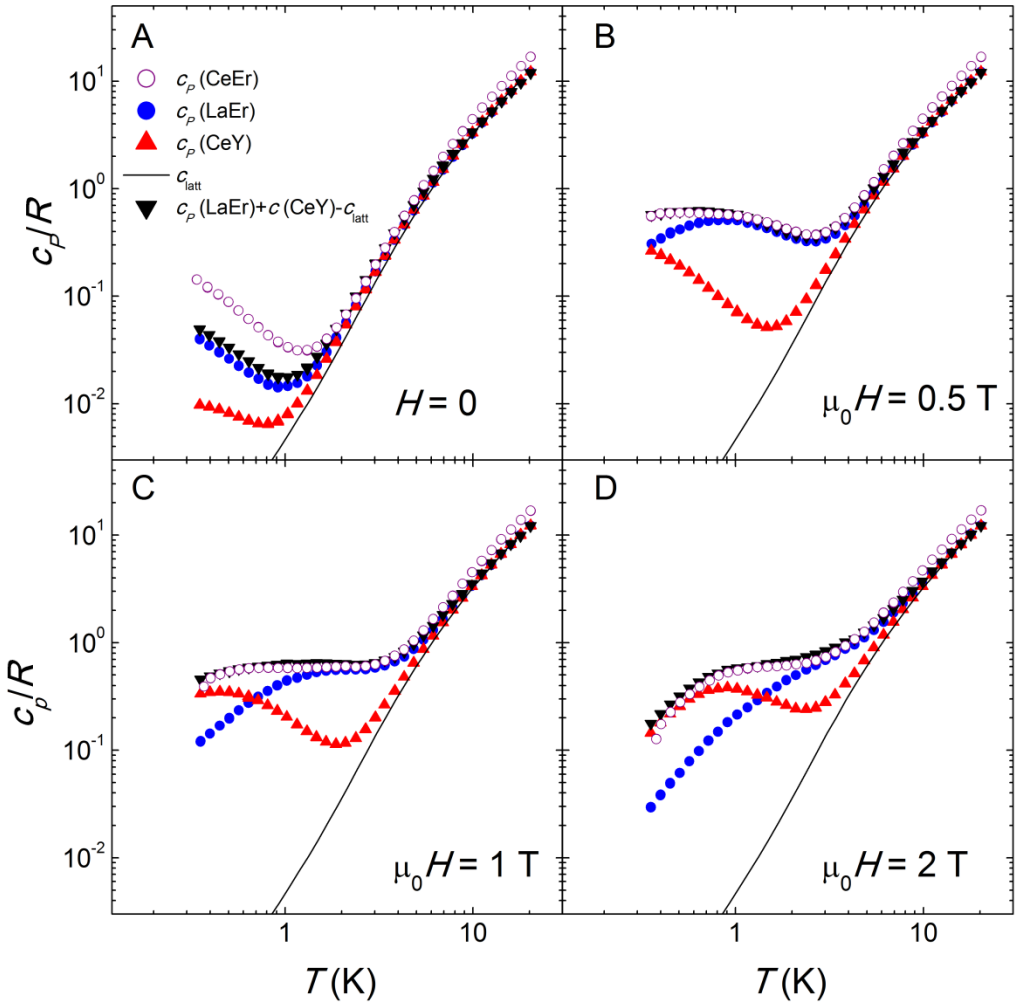


**Figure S17. Heat capacity of coupled qubits.** Specific heat of a powder sample of [CeEr] (**1**) measured at four different magnetic field values, compared to the specific heats of each of the two ions and to that of its sum.

Table S1. Crystallographic data for **1**, **4**, **5**, **6** and **7**.

| Compound | **1**·5py | **4**·5.5py | **5**·5py | **6**·5py | **7**·3py |
|---|---|---|---|---|---|
| Formula | $C_{75}H_{60}CeErN_{10}O_{19}$ | $C_{77.5}H_{62.5}ErLaN_{10.5}O_{19}$ | $C_{75}H_{60}CeN_{10}O_{19}Y$ | $C_{75}H_{57}Ce_{0.70}N_{10}O_{19}Y_{1.30}$ | $C_{65}H_{50}LaN_8O_{19}Y$ |
| FW, g/mol | 1712.71 | 1751.04 | 1634.36 | 1615.97 | 1474.95 |
| $\lambda$, Å | 0.71073 | 0.7749 | 0.7749 | 0.71073 | 0.71073 |
| crystal system | | | monoclinic | | |
| space group | | | $P2_1/c$ | | |
| *a*, Å | 14.5502(3) | 14.5226(11) | 14.450(3) | 14.4500(10) | 14.465(2) |
| *b*, Å | 15.8974(3) | 15.8712(11) | 15.827(3) | 15.867(2) | 15.9220(10) |
| *c*, Å | 35.5552(9) | 35.345(2) | 35.468(6) | 35.483(3) | 35.520(3) |
| $\beta$, deg | 112.521(2) | 112.646(2) | 112.707(6) | 110.535(7) | 111.570(10) |
| *V*, Å$^3$ | 7597.1(3) | 7518.6(9) | 7483(2) | 7618.5(13) | 7607.8(13) |
| *Z* | 4 | 4 | 4 | 4 | 4 |
| $\rho_{cal}$, g/cm$^3$ | 1.497 | 1.546 | 1.451 | 1.409 | 1.288 |
| $\mu$, mm$^{-1}$ | 1.765 | 2.176 | 1.002 | 1.474 | 1.380 |
| *T*, K | 150(2) | 100(2) | 100(2) | 150(2) | 150(2) |
| unique reflections | 12933 | 14111 | 8403 | 7964 | 9231 |
| parameters / restraints | 940 / 206 | 1006 / 371 | 1097 / 697 | 932 / 347 | 923 / 559 |
| w$R_2$[all data] | 0.1208 | 0.2003 | 0.1650 | 0.2721 | 0.2334 |
| $R_1$ (all data) | 0.1170 | 0.0932 | 0.0779 | 0.1739 | 0.1576 |
| w$R_2$ [$I>2\sigma(I)$] | 0.1101 | 0.1959 | 0.1515 | 0.2243 | 0.1968 |
| $R_1$ [$I>2\sigma(I)$] | 0.0569 | 0.0838 | 0.0583 | 0.0973 | 0.0853 |
| *S* [all data] | 0.926 | 1.173 | 1.015 | 1.022 | 1.000 |

CCDC numbers; 973881-973885 for compounds **1**, **4**, **5**, **6** and **7**, respectively.

Table S2. Selected bond distances (Å) and angles (º) of the structures of **1**, **4**, **5**, **6** and **7**.

| compound | **1**·5py (Ln1=Er, Ln2=Ce) | **4**·5.5py (Ln1=Er, Ln2=La) | **5**·5py (Ln1=Y, Ln2=Ce) | **6**·5py (Ln1=Y, Ln2 = Ce / Y) | **7**·3py (Ln1=Y, Ln2=La) |
|---|---|---|---|---|---|
| Ln1–O4 | 2.312(5) | 2.313(7) | 2.319(6) | 2.306(10) | 2.336(8) |
| Ln1–O11 | 2.317(5) | 2.314(7) | 2.323(6) | 2.301(11) | 2.308(8) |
| Ln1–O8 | 2.329(6) | 2.339(7) | 2.332(6) | 2.302(12) | 2.335(8) |
| Ln1–O19 | 2.392(6) | 2.405(8) | 2.401(6) | 2.444(10) | 2.426(9) |
| Ln1–O9 | 2.400(5) | 2.396(7) | 2.397(6) | 2.355(11) | 2.401(8) |
| Ln1–O3 | 2.401(5) | 2.395(7) | 2.396(5) | 2.393(11) | 2.415(9) |
| Ln1–O13 | 2.425(5) | 2.412(6) | 2.423(6) | 2.416(12) | 2.423(8) |
| Ln1–N3 | 2.447(6) | 2.439(8) | 2.443(7) | 2.413(14) | 2.463(10) |
| Ln1–N4 | 2.652(7) | 2.665(9) | 2.674(8) | 2.675(14) | 2.691(10) |
| Ln2–O6 | 2.458(5) | 2.469(7) | 2.448(6) | 2.406(17) / 2.47(5) | 2.450(9) |
| Ln2–O14 | 2.460(5) | 2.474(7) | 2.453(6) | 2.461(16) / 2.33(5) | 2.474(9) |
| Ln2–O1 | 2.480(5) | 2.503(7) | 2.456(6) | 2.380(18) / 2.53(5) | 2.488(10) |
| Ln2–O13 | 2.534(5) | 2.551(7) | 2.518(6) | 2.576(15) / 2.34(4) | 2.575(9) |
| Ln2–O8 | 2.568(5) | 2.574(7) | 2.550(6) | 2.545(16) / 2.49(5) | 2.586(8) |
| Ln2–O16 | 2.597(6) | 2.642(8) | 2.608(6) | 2.474(17) / 2.66(5) | 2.642(10) |
| Ln2–N2 | 2.609(7) | 2.639(9) | 2.621(7) | 2.560(19) / 2.65(5) | 2.605(11) |
| Ln2–O3 | 2.679(5) | 2.687(7) | 2.677(5) | 2.688(15) / 2.53(5) | 2.707(8) |
| Ln2–N1 | 2.722(6) | 2.745(9) | 2.732(6) | 2.711(17) / 2.70(6) | 2.753(11) |
| Ln2–O17 | 2.843(7) | 2.774(10) | 2.812(7) | 2.87(2) / - | 2.807(11) |
| Ln1···Ln2 | 3.8505(6) | 3.8572(7) | 3.8516(11) | 3.879(10)/ 3.69(4) | 3.8693(14) |
| Ln1–O3–Ln2 | 98.43(18) | 98.6(2) | 98.63(18) | 99.4(5) / 97.0(12) | 98.0(3) |
| Ln1–O8–Ln2 | 103.6(2) | 103.4(3) | 104.1(2) | 106.2(5) / 100.7(9) | 103.6(3) |
| Ln1–O13–Ln2 | 101.9(2) | 102.0(2) | 102.4(2) | 101.9(5) / 101.7(14) | 101.4(3) |